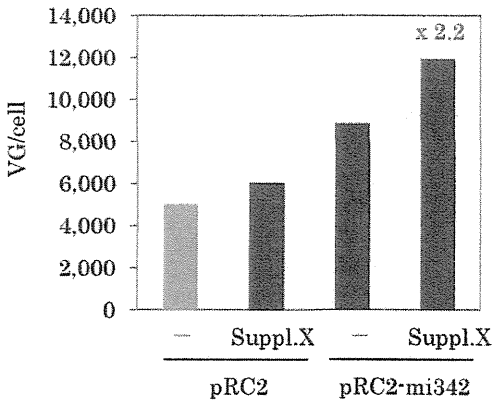

図 1 AAV2 型ベクター製造における hsa-miR342 と Suppl.X の効果

hsa-miR342 は、AAV2 型のヘルパープラスミドに発現ユニットを組み込む形で供給しており、AAV8 型ベクターでの効果を確認するために、AAV8 型のヘルパープラスミドの同じ位置に発現ユニットを組み込んだものを構築した（pRC8-mi342）。また、Suppl.X は AAV2 型の時と同様に、別のプラスミドで供給した。これらにより、AAV8 型ベクターの産生効率を確認したところ、hsa-miR342 については、増強効果が確認できなかったものの、Suppl.X については、約 1.5 倍程度上昇させる作用が認められた（図 2、図 3）。

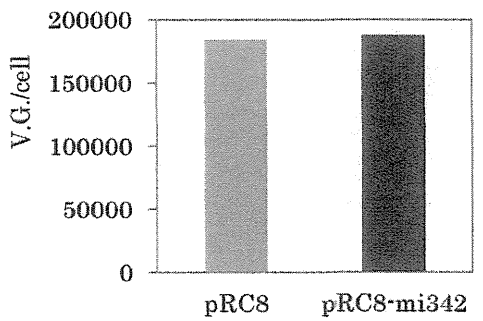

図 2 AAV8 型ベクター製造における hsa-miR342 の効果

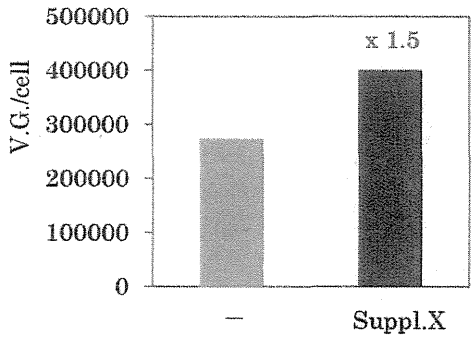

図 3 AAV8 型ベクター製造における Suppl.X の効果

AAV ベクターの製造において、治療用遺伝子を搭載した場合に、蛍光タンパク遺伝子搭載時と比較して、その産生効率が低下することがある。このため、実際の製造スケールを想定するためには、治療用遺伝子、本研究においては FactorIX 遺伝子を搭載した AAV ベクタープラスミドを用いて検討する必要がある。そこで、FactorIX 遺伝子搭載 AAV ベクタープラスミドと AAV8 型ヘルパープラスミド pRC8 を用いて、AAV8-FIX の産生効率を確認したところ、AcGFP 搭載 AAV ベクタープラスミドを使用した場合と比較して、約 1/7 程度に産生効率が低下することが確認された（図 4）。

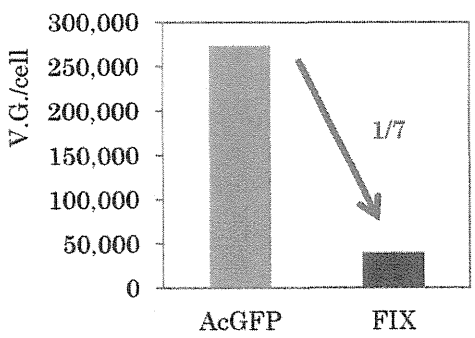

図 4 AcGFP 遺伝子と FactorIX 遺伝子搭載 AAV ベクタープラスミドによる AAV 産生効率の比較

産生効率が 1/7 に低下すると、同じ量のベクター製造を行うためには、7 倍の製造スケールが必要になる。製造スケールが大きくなることで、製造にかかる人員・経費も飛躍的に増大するため、製造スケールについてはできるだけ小さくすることが必要である。そのため、AAV8 型ベクターの製造検討で産生効率の上昇が確認できた Suppl.X を添加するとともに、省スペースで効率良く細胞を培養できるハイパーフラスコを用いて製造効率を確認した（図 5）。

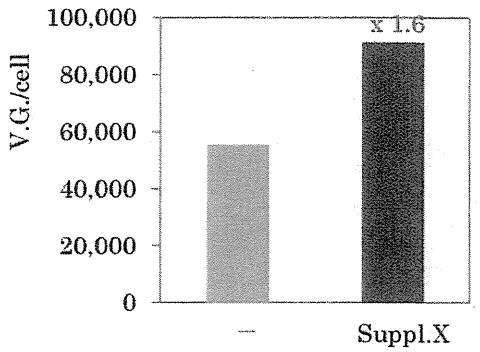

図 5　ハイパーフラスコによる AAV8-FIX 産生

ハイパーフラスコを用いても、通常のフラスコと同等以上の産生効率を示したことから、スケールアップは問題ないことが確認できた。また、Suppl.X の添加により約 1.6 倍程度産生量が増大することも確認できた。そこで、血友病 B に対する遺伝子治療臨床研究を実施する上で必要とされる目標製造量である 1x10^15 vg を製造するための製造スケールについて、これまでの検討をもとに計算した。図 5 の結果から、ハイパーフラスコ 1 個あたり 4x10^12 vg 製造できる計算となり、精製効率を 30%と見積もると、1x10^15 vg を得るためには、ハイパーフラスコが約 800 枚必要と想定された。これは 1 週間あたり 40 枚のハイパーフラスコを処理したとしても 20 週間、約 4 ヶ月強かかることになる。1 週間に 40 枚のハイパーフラスコを処理していくためには、細胞を拡大、準備することも考えると、2 人がかりでほぼかかりきりになって作業しなければいけないこととなる。また、ハイパーフラスコ 1 枚あたりトランスフェクションするプラスミド量として約 200μg 必要であり、800 枚分では 160mg、しかも 4 種類のプラスミド全てについて製造する必要がある。

・バキュロウイルスベクターシステムによる AAV ベクター製造検討：より AAV ベクター製造効率のよい方法を構築するためにバキュロウイルスベクターシステムを利用した製造方法を検討した。既報の文献情報（Mol. Ther., 17(11), 1886-1896, 2009）を参考に、ITR 間に蛍光タンパク AsRed2 遺伝子発現ユニットを配置した AAV ベクターゲノム搭載トランスファーベクター（pBP-AAV）、ならびに Rep と Cap 遺伝子（AAV2 型）を昆虫由来プロモーター下に逆方向に配置したトランスファーベクター（pBP-RC2）を構築した。そのベクター構造について、図 6 に示す。

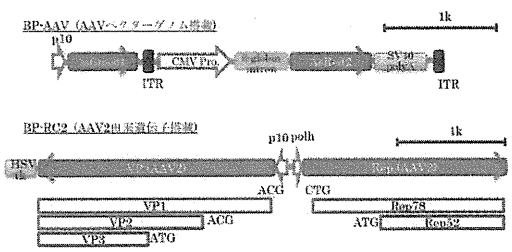

図 6　バキュロウイルスベクター調製用トランスファーベクタープラスミドの構造

それぞれのトランスファーベクターを用いて、それぞれの配列をゲノム内に保持するバキュロウイルスベクター（rBP-AAV 及び rBP-RC2）を調製した。AAV ベクターを調製するためには、これら 2 種類のバキュロウイルスベクターを同時に昆虫細胞に感染させることで行うが、AAV ベクターが実際に産生していることを確認するためには、細胞に感染させたバキュロウイルスベクターを失活させる必要がある。そこで、バキュロウイルスベクターを失活させる効果があるクロロホルムにより粗ウイルス溶液を処理後、ベクターゲノムを測定することで、AAV ベクターが産生しているかどうかを評価した。なお、AAV ベクターはクロロホルムに対して抵抗性があることが知られている。また、コントロールとして、rBP-AAV 単独感染群を設定した。その結果を図 7 に示す。

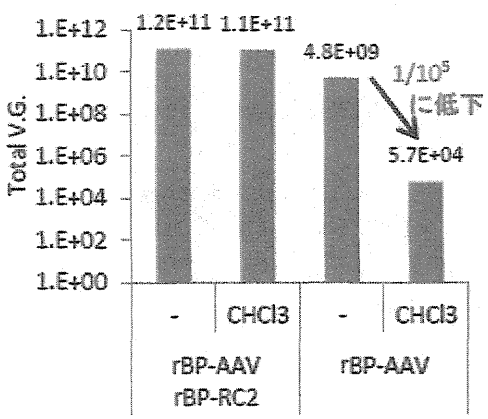

図 7　バキュロウイルスベクターによる AAV ベクター産生の確認

コントロールとして実施した rBP-AAV 単独感染群（AAV ベクターゲノムを保持するバキュロウイルスベクターのみが存在する状態）において、クロロホルムで処理することにより、ベクターゲノム量は $1/10^5$（0.001%）にまで低下しており、このクロロホルム処理によって、バキュロウイルスベクターは効率的に失活できていることが確認できた。一方で、rBP-AAV と rBP-RC2 感染群においては、クロロホルム処理によってもベクターゲノム量の減少はほとんど観察されず、クロロホルム耐性の AAV ベクターが産生していることが示唆された。

次にこのようにして得られた粗ウイルス溶液を、AAV ベクターの精製法としては常法である塩化セシウム密度勾配超遠心により簡易的に精製を試みた。その結果、ヘルパーフリーシステムで調製した AAV ベクターとほぼ同じ RI（Refractory Index）のところに集積が確認できた（図 8）。

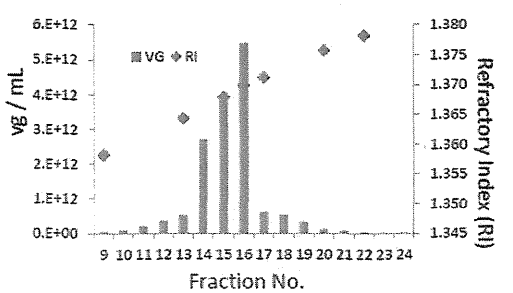

図 8　粗ウイルス液の塩化セシウム密度勾配超遠心精製

AAV ベクターの集積が見られた Fr.14-17 を回収し、透析することにより、精製 AAV ベクター溶液を得た。この精製 AAV ベクターを SDS-PAGE により分析したところ、キャプシドの構成タンパクである VP1、VP2、VP3 が期待される比率で確認できた（図 9）。

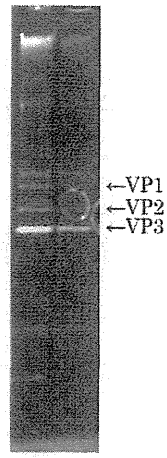

図 9
精製 AAV ベクターの SDS-PAGE による解析

さらに、得られた AAV ベクターの感染性を確認するため、AAV293 細胞に感染させ、3 日後に蛍光顕微鏡により観察した（図 10）。

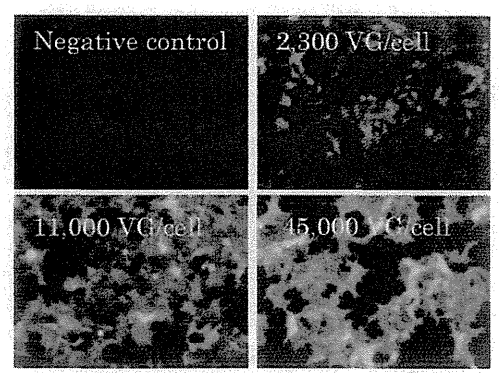

図 10　精製 AAV ベクター（AAV2-AsRed2）の AAV293 細胞への感染性の確認

図 10 に示すように、精製した AAV ベクター（AAV2-AsRed2）は、細胞に感染し、搭載した AsRed2 遺伝子の発現が確認できた。本システムにより得られた AAV ベクター製造量は、6x10^12vg/L であり、目標製造量である 1x10^15 vg を得るためには、200L 程度の培養を行えば確保できるものと考えられた。

D. 考察

血友病 B に対する FactorIX 搭載 AAV ベクターによる遺伝子治療は、最近、海外グループによって有望な成果が報告された（N. Engl. J. Med., 365(25), 2357-2365, 2012）。その中で効果が期待できる投与量は 2x10^12vg/kg であることが示されたが、これは体重 50kg のヒトで 1x10^14vg/kg となり、今後、本邦で同様の遺伝子治療臨床研究を実施するためには、少なくとも 1x10^15vg 程度の GMP 準拠で製造した AAV ベクターが必要と考えられる。

AAV ベクターの製造法には種々の方法が知られているが、なかでもアデノウイルスやヘルペスウイルスなどのヘルパーウイルスを使用しないヘルパーフリーシステムによる製造法は広く用いられている。実際に前述の海外グループによる遺伝子治療においても、ヘルパーフリーシステムによって治療用ベクターが製造された。しかしながら、彼らの文献によると、セルスタック 10 段フラスコを 400 個以上使用して製造したことが記載されており、そのまま同じように製造するには大変な労力を必要とすることが予想された。そこで、できるだけ製造スケールを小さくすることを考え、これまでタカラバイオが蓄積した AAV ベクター産生効率を上昇させるための技術について検討を行った上で、セルスタック 10 段フラスコよりは取扱いが容易なハイパーフラスコを用いて、製造検討を実施した。しかしながら、それでも 1x10^15vg 程度製造するには、ハイパーフラスコが 800 個程度必要であることが試算され、これは、2 人がほぼかかりきりで 4 ヶ月以上作業することになり、

さらにはこの製造には160mg×4種類のプラスミドを調製する必要があることとなる。現実的な問題として、この方法による製造はとてもコストが高くなり、詳細な試算は行っていないが、おそらく1回の製造あたり1億円以上は間違いなく必要と考えられた。また、このようにしてコストをかけて力ずくで今回は製造を行ったとしても、得られるベクター量としては数名分であり、さらなる第Ⅱ相の臨床研究や治験等を見据えた時には、その継続性という観点からも、根本的に解決すべき問題と考えられたため、遺伝子治療用 AAV ベクター製造で実績があるバキュロウイルスベクターを用いた製造システムについて、製造技術開発を行うこととした。

文献情報を参考に、製造系を構築しAAVベクター産生性について確認したところ、200L程度の培養により1x10^15vg程度生産できる可能性が示唆された。バキュロウイルスベクターによる AAV ベクター製造については知識、技術、ノウハウがまだあまり蓄積されていないため、今後慎重に検証を進める必要はあるが、ヘルパーフリーシステムによりハイパーフラスコ800枚を用いて製造することと比較すると、より短期間で、より省力的に製造することが可能と考えられ、さらに、必要なプラスミド量は大幅に少なくなるため、コストは当然下がることが予想される。今後、検証を進めるとともに、実際の治療用ベクターであるAAV8-FIX を製造するためのバキュロウイルスベクター製造系を構築し、その生産性を早急に確認する必要があると考えられる。その上で、GMP製造可能な製造システムの構築、大量ベクターの精製方法の検討を行い、その進捗状況によって、ベクター産生細胞となる昆虫細胞のマスターセルバンク（MCB）の作製及び AAV ベクター製造のためのバキュロウイルスマスターウイルスバンク（MVB）の作製検討へと進めていきたい。

E. 結論

本研究において、血友病Bに対する遺伝子治療臨床研究用ベクター製剤AAV8-FIXの大量製造に関する検討を行った。その結果、安定的かつ継続的な大量製造が可能と考えられるバキュロウイルスベクターによるAAVベクター製造システムについて開発検討を進めることが、最も適当と考えられるだけの結果を得た。今後、臨床用ベクターの産生性等を確認し、その実現可能性を検証するとともに、GMP製造のためのMCB、MVB作製等へと進めていく予定である。

G. 研究発表

なし

H. 知的財産権の出願・登録状況

なし

研究成果の刊行に関する一覧表

雑誌

発表者氏名	論文タイトル名	発表誌名	巻号	ページ	出版年
Sakata A, Ohmori T, Nishimura S, Suzuki H, Madoiwa S, Mimuro J, Kario K, Sakata Y.	Paxillin is an intrinsic negative regulator of platelet activation in mice.	Thromb J		Epub ahead of print	2014
Koyama K, Madoiwa S, Nunomiya S, Koinuma T, Wada M, Sakata A, Ohmori T, Mimuro J, Sakata Y.	Combination of thrombin-antithrombin complex, plasminogen activator inhibitor-1, and protein C activity for early identification of severe coagulopathy in initial phase of sepsis: a prospective observational study.	Criti care		Epub ahead of print	2014
Kashiwakura Y, Ohmori T, Mimuro J, Madoiwa S, Inoue M, Hasegawa M, Ozawa K, Sakata Y.	Production of functional coagulation factor VIII from iPSCs using a lentiviral vector.	Haemophilia	20	e40-e44	2014
Watanabe H, Kikkawa I, Madoiwa S, Sekiya H, Hayasaka S, Sakata Y.	Changes in Blood Coagulation-Fibrinolysis Markers By Pneumatic Tourniquet During Total Knee Joint Arthroplasty With Venous Thromboembolism.	J Arthroplasty	29	569-573	2014
Mimuro J, Mizukami H, Shima M, Matsushita T, Taki M, Muto S, Higasa S, Sakai M, Ohmori T, Madoiwa S, Ozawa K, Sakata Y.	The prevalence of neutralizing antibodies against adeno-associated virus capsids is reduced in young Japanese individuals.	J Med Virol		Epub ahead of print	2013
Yasumoto A, Madoiwa S, Kashiwakura Y, Ishiwata A, Ohmori T, Mizukami H, Ozawa K, Sakata Y, Mimuro J.	Overexpression of factor VII ameliorates bleeding diathesis of factor VIII-deficient mice with inhibitors.	Thromb Res	131	444-449	2013
Mimuro J, Mizukami H, Hishikawa S, Ikemoto, T, Ishiwata A, Sakata, A, Ohmori T, Madoiwa S, Ono F, Ozawa K, Sakata Y.	Minimizing the inhibitory effect of neutralizing antibody for efficient gene expression in the liver with adeno-associated virus 8 vectors.	Mol Ther	21	318-323	2013
Watanabe N, Ohashi K, Tatsumi K, Utoh R, Shim IK, Kanegae K, Kashiwakura Y, Ohmori T, Sakata Y, Inoue M, Hasegawa M, Okano T.	Genetically modified adipose tissue-derived stem/stromal cells, using simian immunodeficiency virus-based lentiviral vectors, in the treatment of hemophilia B.	Hum Gene Ther.	24 (3)	283-294	2013

発表者氏名	論文タイトル名	発表誌名	巻号	ページ	出版年
Madoiwa S, Kitajima I, Ohmori T, Sakata Y, Mimuro J.	Distinct reactivity of the commercially available monoclonal antibodies of D-dimer and plasma FDP testing to the molecular variants of fibrin degradation products.	Thromb Res	132	457-464	2013
Koyama K, Madoiwa S, Tanaka S, Koinuma T, Wada M, Sakata A, Ohmori T, Mimuro J, Nunomiya S, Sakata Y.	Evaluation of hemostatic biomarker abnormalities that precede platelet count decline in critically ill patients with sepsis.	J Crit care	28	556-563	2013
Takahashi K, Mizukami H, Saga Y, Takei Y, Urabe M, Kume A, Machida S, Fujiwara H, Suzuki M, Ozawa K.	Suppression of lymph node and lung metastases of endometrial cancer by muscle-mediated expression of soluble vascular endothelial growth factor receptor-3.	Cancer Sci	104	1107-11	2013
Shimada M, Abe S, Takahashi T, Shiozaki K, Okuda M, Mizukami H, Klinman D.M, Ozawa K, Okuda K.	Prophylaxis and treatment of Alzheimer's disease by delivery of an adeno-associated virus encoding a monoclonal antibody targeting the amyloid Beta protein.	PLoS One	8	e57606	2013
Muto A, Yoshihashi K, Takeda M, Kitazawa T, Soeda T, Igawa T, Sakamoto Y, Haraya K, Kawabe Y, Shima M, Yoshioka A, Hattori K.	Anti-factor IXa/X bispecific antibody (ACE910): hemostatic potency against ongoing bleeds in a hemophilia A model and the possibility of routine supplementation.	J Thromb Haemost	12	206-213	2014
Tatsumi K, Sugimoto M,Lillicrap D, Shima M, Ohashi K, Okano T, Matsui H.	A Novel Cell-Sheet Technology That Achieves Durable Factor VIII Delivery in a Mouse Model of Hemophilia A.	PLoS One	8(12)	e83280	2013
Shima M.	Hemophilia world.	Rinsho Ketsueki	54 (8)	736-43	2013
Yada K, Nogami K,Shima M.	Different factor VIII neutralizing effects on anti-factor VIII inhibitor antibodies associated with epitope specificity and von Willebrand factor.	Br J Haematol	163 (1)	104-11	2013

発表者氏名	論文タイトル名	発表誌名	巻号	ページ	出版年
Sakurai Y, Kasuda S, Tatsumi K, Takeda T, Kato J, Kubo A, Shima M.	Repression of Factor VIII Inhibitor Development with Apoptotic Factor VIII-expressing Embryonic Stem Cells.	Hematol Rep	5(2)	30-3	2013
Kajiwara M, Shima M, Yoshioka A.	Two haemophilia patients with inhibitors who became ambulatory after physiotherapy under haemostatic cover with bypassing agents.	Haemophilia	19(5)	e301-4	2013
Shima M, Thachil J, Nair SC, Srivastava A.	Towards standardization of clot waveform analysis and recommendations for its clinical applications.	J Thromb Haemost	11(7)	1417-20	2013
Doi M, Sugimoto M, Matsui H, Matsunari Y, Shima M.	Coagulation potential of immobilised factor VIII in flow-dependent fibrin generation on platelet surfaces.	Thromb Haemost	110 (2)	316-22	2013
Shima M.	Hemophilia.	Rinsho Ketsueki	54(2)	189-97	2013
Yada K, Nogami K, Wakabayashi H, Fay PJ, Shima M.	The mild phenotype in severe hemophilia A with Arg1781His mutation is associated with enhanced binding affinity of factor VIII for factor X.	Thromb Haemost	109 (6)	1007-15	2013
Inaba H, Shinozawa K, Seita I, Otaki M, Suzuki T, Hagiwara T, Amano K, Fukutake K.	Genotypic and phenotypic features of Japanese patients with mild to moderate hemophilia A.	Int J Hematol.	97	758-64	2013
Iwata N, Sekiguchi M, Hattori Y, Takahashi A, Asai M, Ji B, Higuchi M,Staufenbiel M, Muramatsu S, Saido TC.	Global brain delivery of neprilysin gene by intravascular administration of AAV vector in mice.	Sci Rep	3	1472	2013
Iida A, Takino N, Miyauchi H, Shimazaki K ,Muramatsu S.	Systemic delivery of tyrosine-mutant AAV vectors results in robust transduction of neurons in adult mice.	Bio Med Res Int	2013	974819	2013
Yamashita T, Chai HL, Teramoto S, Tsuji S, Shimazaki K, Muramatsu S, Kwak S.	Rescue of amyotrophic lateral sclerosis phenotype in a mouse model by intravenous AAV9-ADAR2 delivery to motor neurons.	EMBO Mol Med	5	1-10	2013

研究成果の刊行物・別刷

Sakata et al. Thrombosis Journal 2014, 12:1
http://www.thrombosisjournal.com/content/12/1/1

THROMBOSIS JOURNAL

ORIGINAL BASIC RESEARCH Open Access

Paxillin is an intrinsic negative regulator of platelet activation in mice

Asuka Sakata[1,2], Tsukasa Ohmori[1*], Satoshi Nishimura[1,3,4], Hidenori Suzuki[5], Seiji Madoiwa[1], Jun Mimuro[1], Kazuomi Kario[2] and Yoichi Sakata[1]

Abstract

Background: Paxillin is a LIM domain protein localized at integrin-mediated focal adhesions. Although paxillin is thought to modulate the functions of integrins, little is known about the contribution of paxillin to signaling pathways in platelets. Here, we studied the role of paxillin in platelet activation in vitro and in vivo.

Methods and results: We generated paxillin knockdown (Pxn-KD) platelets in mice by transplanting bone marrow cells transduced with a lentiviral vector carrying a short hairpin RNA sequence, and confirmed that paxillin expression was significantly reduced in platelets derived from the transduced cells. Pxn-KD platelets showed a slight increased in size and augmented integrin αIIbβ3 activation following stimulation of multiple receptors including glycoprotein VI and G protein-coupled receptors. Thromboxane A_2 biosynthesis and the release of α-granules and dense granules in response to agonist stimulation were also enhanced in Pxn-KD platelets. However, Pxn-KD did not increase tyrosine phosphorylation or intracellular calcium mobilization. Intravital imaging confirmed that Pxn-KD enhanced thrombus formation in vivo.

Conclusions: Our findings suggest that paxillin negatively regulates several common platelet signaling pathways, resulting in the activation of integrin αIIbβ3 and release reactions.

Keywords: Platelet, Glycoprotein, Platelet aggregation, Release reaction

Background

A breakdown of normal platelet function results in either unexpected bleeding or thrombotic events [1]. Platelets are inactive in the intact vasculature under physiological conditions. However, once the platelets encounter an injured region of the endothelium, they attach through an interaction between von Willebrand factor and the glycoprotein (GP) Ib/IX/V complex [2], and then collagen receptor GPVI triggers platelet activation. Activated platelets release several classes of agonists, including ADP and thromboxane (Tx) A_2, which promote further platelet activation [3]. These steps ultimately increase the affinity of integrin αIIbβ3 for its ligands and induce platelet aggregation [4]. The intracellular signaling that increases the affinity of integrins is known as inside-out signaling [4]. Multiple signal transduction pathways from various receptors share common inside-out signaling cascades. For example, phosphoinositol hydrolysis, which leads to calcium mobilization and protein kinase C activation [5], and Rap1b activation are well-known signaling pathways that regulate integrin-mediated platelet functions [6].

To increase the affinity of integrin αIIbβ3, inside-out signaling pathways induce a drastic conformational change of the integrin [7]. Direct interactions between cytoskeletal proteins (e.g., talin and kindlin) and cytoplasmic β integrin are essential for inducing the conformational change of integrins [7]. Indeed, the loss of talin or kindlin in platelets dramatically reduces integrin αIIbβ3-mediated platelet aggregation, despite normal expression levels of the surface receptors [8,9]. Selective blockade of talin binding by a single amino acid substitution in β3 integrin also impairs integrin αIIbβ3-dependent platelet responses [10]. Although a number of integrin-associated proteins have been reported [11], the identities of proteins and their roles in regulating integrin signaling in platelets have not been fully characterized. It is also unknown whether

* Correspondence: tohmori@jichi.ac.jp
[1]Research Division of Cell and Molecular Medicine, Center for Molecular Medicine, Jichi Medical University School of Medicine, 3111-1 Yakushiji, Shimotsuke, Tochigi 329-0498, Japan
Full list of author information is available at the end of the article

BioMed Central

© 2014 Sakata et al.; licensee BioMed Central Ltd. This is an Open Access article distributed under the terms of the Creative Commons Attribution License (http://creativecommons.org/licenses/by/2.0), which permits unrestricted use, distribution, and reproduction in any medium, provided the original work is properly cited. The Creative Commons Public Domain Dedication waiver (http://creativecommons.org/publicdomain/zero/1.0/) applies to the data made available in this article, unless otherwise stated.

additional molecules, other than talin and kindlin, are capable of regulating integrin signaling pathways.

Paxillin is a LIM domain protein that was originally identified as a substrate for oncogene *v-src* [12]. Paxillin contains two conserved structural domains, the N-terminus and C-terminus, which consist of four LIM domains [13,14]. Two other family members have also been identified, Hic-5 and leupaxin [13,14]. Paxillin is ubiquitously expressed alongside these variants [13,14], except in human platelets that predominantly express Hic-5 [15,16]. Conversely, mouse platelets express paxillin and leupaxin in addition to Hic-5 [17]. Considering the multiple interaction motifs located within its structure, paxillin appears to serve as a signaling platform for the recruitment of numerous regulatory proteins near integrins [13,14]. Paxillin directly interacts with the cytoplasmic domain of integrin α4 and α9, but not αIIb, and these interactions controls integrin-mediated cell migration and spreading [18,19].

Integrin αIIbβ3 in platelets is suitable for studies of integrin receptors because its ligand binding and signal transduction pathways are well characterized. Elucidating the intracellular proteins involved in the activation of integrin αIIbβ3 can provide a better understanding of the functions of integrins and might result in the discovery of new antithrombotic targets [20]. We previously reported that lentiviral vector-mediated short hairpin RNA (shRNA) expression in hematopoietic stem cells greatly reduces the expression of the target protein in platelets [21]. This method enables functional analyses of target proteins that modulate platelet activation in anucleate platelets [21]. In the present study, we used this method to investigate the roles of paxillin in platelet activation, and found that paxillin negatively regulates platelet signaling pathways including the activation of integrin αIIbβ3 and release reactions.

Materials and methods

Materials

All mouse cytokines were purchased from PeproTech (London, UK). The following antibodies and agonists were obtained from the specified suppliers: PAC-1 monoclonal antibody (mAb), anti-mouse P-selectin mAb (RB40.34), anti-paxillin mAb (clone 349), and anti-Hic-5 mAb (BD Biosciences, San Jose, CA); horseradish peroxidase-conjugated anti-green fluorescent protein (GFP) polyclonal antibody (Acris Antibodies, Himmelreich, Germany); phycoerythrin (PE)-Cy7-conjugated anti-mouse IgM (eBioscience, San Diego, CA); anti-talin mAb (clone 8D4); anti-phosphotyrosine mAb (clone 4G10), and BAPTA-AM (Millipore, Billerica MA); human fibrinogen and epinephrine (Sigma-Aldrich, St. Louis, MO); anti-vinculin mAb (V284) (Chemicon, Billerica, MA); anti-mouse GPVI mAb (Six.E10), anti-mouse GPIbα mAb (Xia.G5), and anti-mouse integrin αIIbβ3 mAb (Leo.D2 and clone JON/A) (Emfret Analytics, Eibelstadt, Germany); anti-α-actin mAb (D6F6), anti-FAK polyclonal antibody, and anti-Src mAb (32G6) (Cell Signaling Technology, Danvers, MA); anti-Rap1b polyclonal antibody and anti-protein kinase Cα mAb (M4) (Upstate Cell Signaling Solutions, Lake Placid, NY); allophycocyanin (APC)-conjugated anti-rat IgG polyclonal antibody (R& D Systems, Minneapolis, MN); convulxin (ALEXIS Biochemicals, Plymouth Meeting, PA); AYPGKF (Invitrogen, Carlsbad, CA); ADP (MC medical, Tokyo, Japan); U46619 (Cayman Chemical, Ann Arbor, MI).

Lentiviral vector and virus production

A lentiviral vector plasmid for expression of shRNA sequences and GFP (LentiLox vector) was purchased from the American Type Culture Collection (Manassas, VA) [22]. To efficiently express GFP in platelets, the cytomegalovirus promoter of the LentiLox vectors was substituted with the platelet-specific GPIbα promoter (LentiLox-GPIbα) [21]. Putative shRNA sequences were designed using web-based software provided by Thermo Scientific Molecular Biology (http://www.thermoscientificbio.com/design-center/). Three shRNA sequences were synthesized for mouse paxillin and then cloned into a LentiLox vector plasmid (Additional files 1 and 2). Lentiviruses were produced as described previously [23].

Transplantation of mouse bone marrow cells

All animal procedures were approved by the Institutional Animal Care and Concern Committee of Jichi Medical University, and animal care was performed in accordance with the committee's guidelines. Mouse bone marrow cells (C57BL/6 J) were isolated and resuspended in StemPro®-34 SFM medium (Invitrogen) supplemented with 100 ng/mL each of stem cell factor, thrombopoietin, interleukin-6, and fms-like tyrosine kinase 3 ligand, and 200 ng/mL soluble interleukin-6 receptor. The lentiviral vector was added at 12–16 h after cell isolation (multiplicity of infection [MOI] = 5), and the cell culture was continued for 21–22 h. Each recipient mouse (8–12 weeks of age) was irradiated with a single lethal dose of 9.5 Gy and then intravenously injected with 2×10^6 lentivirus-transduced bone marrow cells. After transplantation, about 50% of platelets expressed GFP (Figure 1). Mice with 70% of their platelets exhibiting GFP positivity were used in experiments that could not distinguish GFP-positive platelets, *i.e.*, light transmission aggregometry, clot retraction, release concentration, calcium mobilization, and intravital microscopy.

Immunoblotting

Immunoblotting with the specific antibodies was performed as described previously [21]. To assess protein tyrosine phosphorylation, washed platelets were pretreated

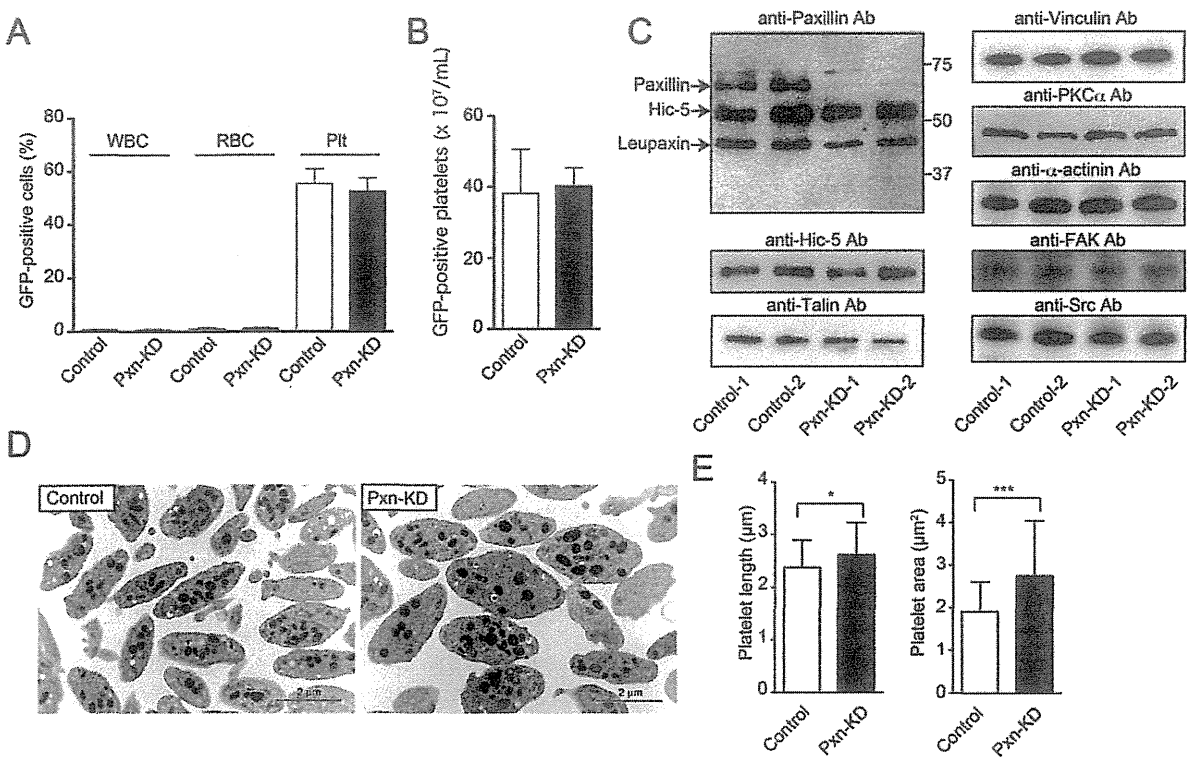

Figure 1 Characterization of Pxn-KD platelets. Bone marrow cells transduced with LentiLox-sh-control-GPIbα (Control) or LentiLox-sh-paxillin-GPIbα (Pxn-KD) at an MOI of 5 were transplanted into lethally irradiated recipient mice. **(A)** The numbers of GFP-positive cells (%) among white blood cells (WBCs), red blood cells (RBCs), and platelets (Plts) in peripheral blood at 30 days after transplantation were assessed by flow cytometry. Columns and error bars represent the mean ± s.d. ($n = 10$). **(B)** Absolute number of GFP-positive platelets in peripheral blood at 30 days after transplantation. Columns and error bars represent the mean ± s.d. ($n = 10$). **(C)** Platelet lysates were immunoblotted with the indicated antibodies. Data are for two mice with >80% of platelets expressing GFP in each experiment. **(D)** The morphology of control and Pxn-KD platelets was examined by transmission electron microscopy. Bars = 2 μm. **(E)** Platelet length (left panel) and area (right panel) were quantified by ImageJ software. Columns and error bars represent the mean ± s.d. ($n = 53–72$). Statistical significance was determined by the Student's *t*-test. $^*P < 0.05$ and $^{***}P < 0.001$ vs. control.

with 1 mmol/L EDTA, 5 U/mL apyrase, and 10 μmol/L SQ29548 to exclude the effects of aggregation, released ADP, and TxA_2.

Transmission electron microscopy

Mouse platelet pellets were fixed in 2% glutaraldehyde in 0.1 mol/L phosphate buffer (pH 7.4) for 60 min at 4°C. The samples were washed, post-fixed with 1% osmium tetroxide in 0.1 mol/L phosphate buffer for 60 min at 4°C, dehydrated with a graded ethanol series, and then embedded in Epon (TAAB Laboratories, Aldermaston, UK) as described previously [24]. Ultrathin sections were prepared, stained with uranyl acetate and lead citrate, and then examined under a JEM1010 transmission electron microscope (JEOL, Tokyo, Japan) at an accelerating voltage of 80 kV. The length and area of platelets were quantified using ImageJ Ver. 10.2 for Macintosh (NIH, Bethesda, MD).

Preparation of washed mouse platelets and flow cytometry

A blood sample (100–400 μL) was drawn from each mouse through the right jugular vein using a 30 G syringe containing 1/10 sodium citrate, and then diluted with 3 mL Hepes/Tyrode buffer (138 mmol/L NaCl, 3.3 mmol/L NaH_2PO_4, 2.9 mmol/L KCl, 1 mmol/L $MgCl_2$, 1 mg/mL glucose, and 20 mmol/L Hepes, pH 7.4). The diluted blood was centrifuged at $120 \times g$ for 8 min, and the platelets obtained from the platelet-rich fraction were washed and resuspended in Hepes/Tyrode buffer. Just prior to centrifugation, a 15% acid-citrate-dextrose A solution and 0.1 μmol/L prostaglandin I_2 were added to inhibit platelet activation. The final platelet suspensions were adjusted to 1×10^7 platelets/mL and supplemented with 1 mmol/L $CaCl_2$. To assess the binding of JON/A, a monoclonal antibody (mAb) that recognizes activated mouse αIIbβ3 [25], to platelets, 30 μL of washed platelets was incubated with 4 μL of agonist solution, 4 μL of phycoerythrin (PE)-

conjugated JON/A and 1 μL of biotin-conjugated anti-mouse P-selectin mAb for 5 min, and then supplemented with 1 μL of allophycocyanin (APC)-conjugated streptavidin. After 15 min of incubation, JON/A binding and P-selectin expression were determined by flow cytometry using a FACSAria Cell Sorter (Becton Dickinson, Mountain View, CA). Antibody binding was quantified as the mean fluorescence intensity (MFI) of GFP-positive platelets.

Platelet aggregation

Washed platelets were prepared as described above. The final suspensions were adjusted to 2×10^8 platelets/mL and supplemented with 1 mmol/L $CaCl_2$ and 200 μg/mL fibrinogen. The aggregation response to agonist stimulation was measured based on light transmission measured using a PA-200 platelet aggregation analyzer (Kowa, Tokyo, Japan).

Measurement of platelet products

Washed platelets (2×10^8/mL) were stimulated with the indicated agonists for 15 min, and then the supernatants were recovered by centrifugation. The levels of platelet factor 4 (PF4) and serotonin in the supernatants were measured using a mouse PF4 enzyme-linked immunosorbent assay (ELISA) kit (R & D Systems) and an anti-serotonin ELISA kit (GenWay Biotech, San Diego, CA), respectively. The levels of TxB_2 in the supernatants were measured using an enzyme immunoassay (Cayman Chemical).

Platelet adhesion

Platelet adhesion to fibrinogen was assessed as described previously [21]. Briefly, eight-well dishes (Lab-Tek® Chamber Slide™) were coated with 400 μg/mL fibrinogen and then blocked with 1 mg/mL bovine serum albumin (BSA). Platelets were then added to the fibrinogen-coated dishes and incubated for 30 min at 37°C. Adherent platelets were fixed with 3% paraformaldehyde and then permeabilized with phosphate-buffered saline (PBS) containing 0.3% Triton X-100 and 5% donkey serum. After washing with PBS, the platelets were incubated with an anti-GFP polyclonal antibody (MBL, Aichi, Japan). Bound antibodies were detected by Alexa Fluor 488-conjugated anti-rabbit IgG. Actin filaments were detected by staining with 1 μg/mL rhodamine-conjugated phalloidin. Immunofluorescence staining was observed and photographed under a confocal microscope (FV1000; Olympus, Tokyo, Japan). The spread area of GFP-positive platelets was quantified using ImageJ software. Because Pxn-KD platelets were slightly larger than control platelets (Figure 1), the mean platelet size determined by BSA staining was subtracted from the total area on fibrinogen to calculate the actual increase in platelet spreading.

Clot retraction

Human platelet-poor plasma was mixed with the same volume of Hepes/Tyrode buffer containing washed mouse platelets (final concentration: 3×10^8 platelets/ml). Plasma coagulation was initiated by addition of 0.1 U/mL thrombin. The clots were photographed at various time points after thrombin addition. When indicated, 0.5 mmol/L manganese was added to exclude the role of inside-out signaling. The two-dimensional area of serum formation extruded by clot retraction was quantified using ImageJ software and expressed as the progression of clot retraction.

Calcium mobilization

Platelets were incubated with GFP-Certified™ FluoForte™ dye (Enzo Life Sciences, Farmingdale, NY). The fluorophore-loaded platelets (2×10^8/mL) were resuspended in Hepes-Tyrode buffer containing 1 mmol/L EDTA, 5 U/mL apyrase, and 10 μmol/L SQ29548 to exclude the effects of aggregation, extracellular calcium, released ADP, and TxA_2. After stimulation, the intracellular calcium concentration was determined by monitoring the fluorescence (excitation, 530 nm; emission, 570 nm) using a microplate spectrofluorometer (Gemini EM; Molecular Devices, Sunnyvale, CA).

Intravital microscopy and thrombus formation

Intravital microscopy was performed to analyze thrombus formation in vivo as reported previously [26]. Briefly, Texas Red-dextran (100 mg/kg body weight [BW], molecular weight: 70 kDa; Invitrogen), Hoechst 33342 (10 mg/kg BW; Invitrogen), Dylight 488-conjugated anti-CD42b antibody (200 μg/kg BW; Emfret), and hematoporphyrin (5 mg/kg BW; Sigma) were injected into anesthetized mice to produce reactive oxygen species (ROS) following laser irradiation. Blood cell dynamics were visualized during laser excitation (wavelengths 405, 488, and 561 nm; 1.5 mW total power at 100× objective lens). After laser irradiation, sequential images of the mesentery were obtained using a resonance scanning confocal microscope (Nikon A1R; Nikon, Tokyo, Japan). The areas of thrombus (shown by anti-CD42b antibody signals) before and after laser irradiation were calculated using NIS-Elements AR 3.2 (Nikon). When indicated, thrombus formation in the femoral artery was triggered by topical application of a filter paper tip saturated with 10% $FeCl_3$. After injection of Texas Red-dextran, Hoechst 33342, and Dylight 488-conjugated anti-CD42b antibody, thrombus formation was visualized and monitored by confocal microscopy using two photon microscopy (excitation wavelength 840 nm) by NikonA1R MP (Nikon).

Bleeding time

The distal tail tip (5 mm) of an anesthetized mouse was clipped, and the tail was immediately immersed in PBS

at 37°C. Tail bleeding times were defined as the time required for the bleeding to stop.

Results

Generation of paxillin knockdown (Pxn-KD) platelets

To address the function of paxillin in mouse platelets, we used a lentiviral vector carrying shRNA sequences and GFP [22]. We synthesized three shRNA sequences for mouse paxillin, and cloned them into a LentiLox vector plasmid (Additional files 1 and 2). We selected one sequence that significantly inhibited paxillin expression in embryonic fibroblasts after transduction (Pxn-1 sequence; Additional files 1 and 2). After transplantation of bone marrow cells transduced with either the control or Pxn-KD sequence, about 50% of the platelets expressed GFP, and the absolute numbers of GFP-positive platelets did not differ between experiments using control and Pxn-KD sequences (Figure 1A–B). Furthermore, there was no effect on the total number of platelets (control: $6.8 \pm 1.72 \times 10^8$/mL; Pxn-KD: $7.7 \pm 0.65 \times 10^8$/mL, $P = 0.18$). We compared the platelet aggregation response and release reaction in platelets from wild-type C57BL/6 J and control mice, and confirmed that platelet aggregation as well as the release reaction did not differ (data not shown). To confirm knockdown of paxillin in GFP-positive platelets, we selected mice in which more than 80% of platelets expressed GFP after transplantation. Immunoblotting of platelet lysates with an anti-paxillin mAb (clone 349) showed a marked reduction in paxillin expression following transplantation of bone marrow cells transduced with the Pxn-KD sequence (Figure 1C). This antibody also recognizes other members of the paxillin family, including Hic-5 and leupaxin [17]. However, Hic-5 and leupaxilin were not affected by expression of the Pxn-KD sequence (Figure 1C). Transmission electron microscopy of resting platelets revealed that the Pxn-KD platelets were slightly larger than control platelets (Figure 1D–E). This change was largely dependent on an increase of the cytoplasm volume, but not the granule volume (Additional file 3). Pxn-KD platelets showed marginally elevated expression levels of GPIb and integrin αIIbβ3, even though GPVI expression was normal (Additional file 4). These changes in Pxn-KD platelets were supposed to result from the increase in platelet size.

Augmentation of integrin αIIbβ3 activation in Pxn-KD platelets

We first focused on the role of paxillin in integrin αIIbβ3 activation that is critical for platelet aggregation. We performed flow cytometric analysis of integrin αIIbβ3 activation using an anti-JON/A mAb [25]. GFP-positive Pxn-KD platelets (Figure 2A, lower panel) showed significantly enhanced αIIbβ3 activation following stimulation compared with that of control platelets (Figure 2A, upper panel). Enhanced JON/A binding of Pxn-KD platelets was observed following stimulation with the GPVI agonist convulxin and G protein-coupled receptor agonists including a protease-activated receptor 4 agonist (AYPGKF), ADP, and U46619 (Figure 2A–B). However, JON/A binding was not enhanced in unstimulated or epinephrine-stimulated platelets, suggesting that Pxn-KD alone does not induce activation of integrin αIIbβ3. We next used light transmission aggregometry to assess platelet aggregation in vitro. We found that platelet aggregation was significantly augmented in Pxn-KD platelets, and this effect was evident at low agonist concentrations that induce platelet aggregation (Figure 2C–D).

Enhanced release reactions and Tx biosynthesis in Pxn-KD platelets

We next assessed the release reactions in response to stimulation. To address the role of paxillin in α-granule secretion, P-selectin expression was determined in GFP-positive platelets by flow cytometry. As shown in Figure 3A–B, P-selectin expression in Pxn-KD platelets was significantly increased following stimulation with convulxin, AYPGKF, and U46619. In contrast, P-selectin expression was not increased by stimulation with ADP or epinephrine. We observed negligible increases in P-selectin expression of Pxn-KD platelets under the resting condition and after incubation with the fibronectin peptide Gly-Arg-Gly-Asp-Ser (GRGDS) (Figure 3B). To examine whether Pxn-KD platelets are already activated during circulation, we compared P-selectin expression in washed platelets and whole blood platelets before the preparation. An increase of P-selectin expression after washing the platelet preparation was observed in Pxn-KD platelets (30.0 ± 9.71 to 37.2 ± 5.72 in the control vs. 27.8 ± 2.56 to 44.8 ± 7.87, $P < 0.05$), suggesting that the susceptibility of Pxn-KD platelets caused marginal activation during washing. Although PF4 and serotonin content in resting platelets did not differ between control and Pxn-KD platelets (Additional file 3), the actual release of PF4 and serotonin into the supernatant in response to platelet activation was also enhanced in Pxn-KD platelets (Figure 3C–D). Of note, a marked increase in TxB_2 biosynthesis was observed in Pxn-KD platelets (Figure 3E). Pretreatment with the ADP scavenger apyrase and thromboxane A_2 receptor antagonist SQ29548 somewhat corrected the increase of JON/A binding in Pxn-KD platelets. This result suggests that the extent of the increase of integrin activation is partially dependent on the release reaction (Additional file 5). Collectively, these data suggest that paxillin negatively regulates platelet activation signaling pathways leading to integrin activation, release reactions, and Tx synthesis. It is possible that general pathway (s) involved in platelet activation were enhanced by Pxn-KD, because platelet activation was increased in

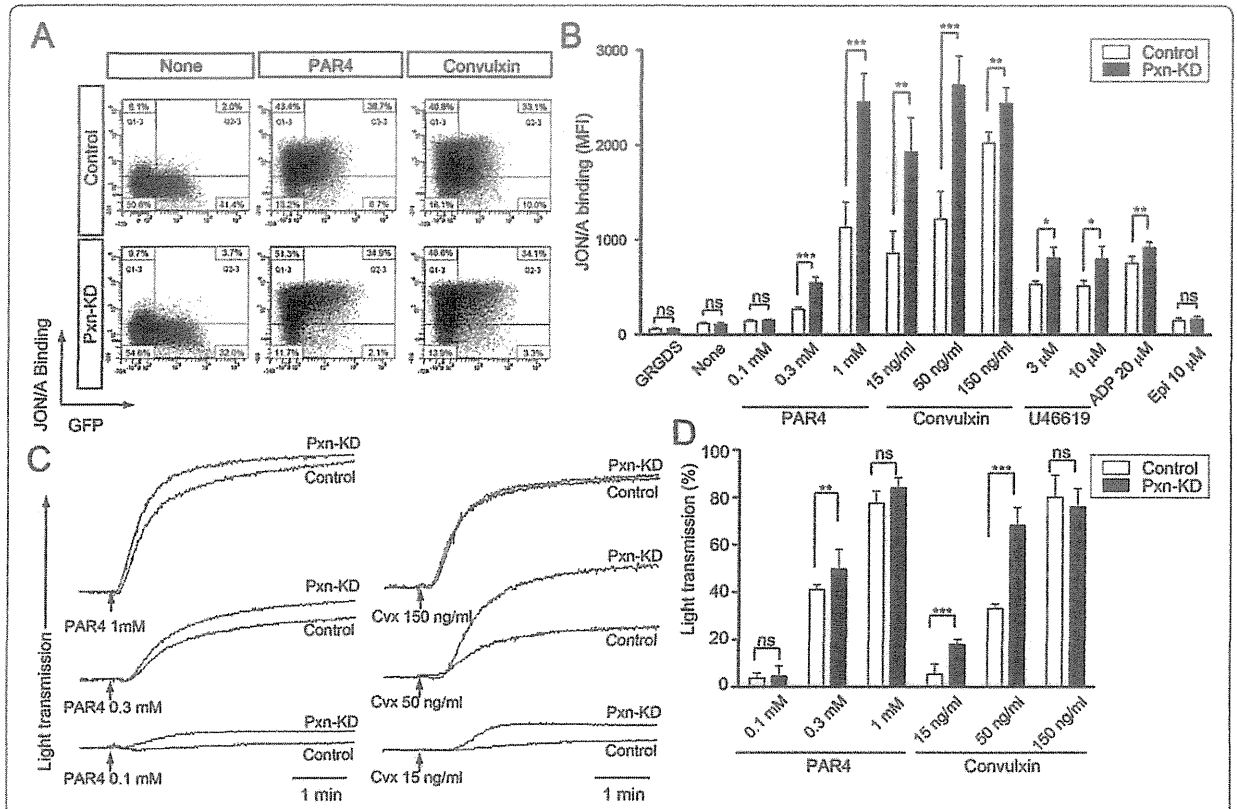

Figure 2 Pxn-KD in platelets increases agonist-induced integrin αIIbβ3 activation. Bone marrow cells transduced with LentiLox-sh-control-GPIbα (Control) or LentiLox-sh-paxillin-GPIbα (Pxn-KD) at an MOI of 5 were transplanted into lethally irradiated recipient mice. **(A)** Activation of integrin αIIbβ3 was assessed by JON/A binding to platelets incubated with or without 1 mmol/L AYPGKF or 50 ng/mL convulxin. The plots represent the degree of GFP expression (horizontal) and binding of JON/A, a monoclonal antibody that recognizes activated integrin αIIbβ3 (vertical). **(B)** Columns and error bars represent the mean ± s.d. of the MFI of JON/A binding after stimulating GFP-positive platelets with the indicated agonists ($n = 3–5$). **(C)** Platelet aggregation induced by the indicated concentration of AYPGKF or convulxin was monitored by light transmission aggregometry. **(D)** Columns and error bars represent the mean ± s.d. of maximal platelet aggregation after stimulation ($n = 5$). Open bars: control platelets; black bars: Pxn-KD platelets. Statistical significance was determined by the Student's *t*-test. $^*P < 0.05$, $^{**}P < 0.01$, and $^{***}P < 0.001$.

response to several classes of activators including GPVI and G protein-coupled receptors.

Assessment of outside-in signaling pathways in Pxn-KD platelets

To address the role of paxillin in outside-in signaling of integrin αIIbβ3, we assessed platelet spreading on fibrinogen and clot retraction. The cell area independent of integrin outside-in signaling (i.e., adherent to the BSA control) was slightly increased in Pxn-KD platelets compared with that in control platelets (data not shown), because the Pxn-KD platelets were marginally larger than control platelets (Figure 1). To quantify the increase in platelet spreading, the mean platelet size on BSA was subtracted from the total spreading area on fibrinogen. As shown in Figure 4A, the increase in platelet spreading on fibrinogen without or with convulxin stimulation was significantly greater for Pxn-KD platelets than that for control platelets (Figure 4A–B). In addition, clot retraction induced by thrombin was significantly enhanced in Pxn-KD platelets compared with that in control platelets (Figure 4C–D). Acceleration of clot retraction in Pxn-KD platelets was also observed in the presence of manganese at 15 min (6.98 ± 0.130 vs. 7.56 ± 0.072, $P < 0.05$). These observations suggest that paxillin is an important regulator of integrin outside-in signaling via integrin αIIbβ3.

The role of paxillin in calcium mobilization in platelets

Because GPVI initiates signaling cascades by activation of non-receptor tyrosine kinases, we assessed tyrosine phosphorylation elicited by the GPVI signaling pathway. As a result, tyrosine phosphorylation events induced by convulxin were not affected by Pxn-KD (Figure 5A). The agonist-induced increase in intracellular calcium mobilization is an important common and proximal signaling event controlling platelet activation. Therefore, we next examined whether Pxn-KD enhanced intracellular calcium mobilization following stimulation. To exclude

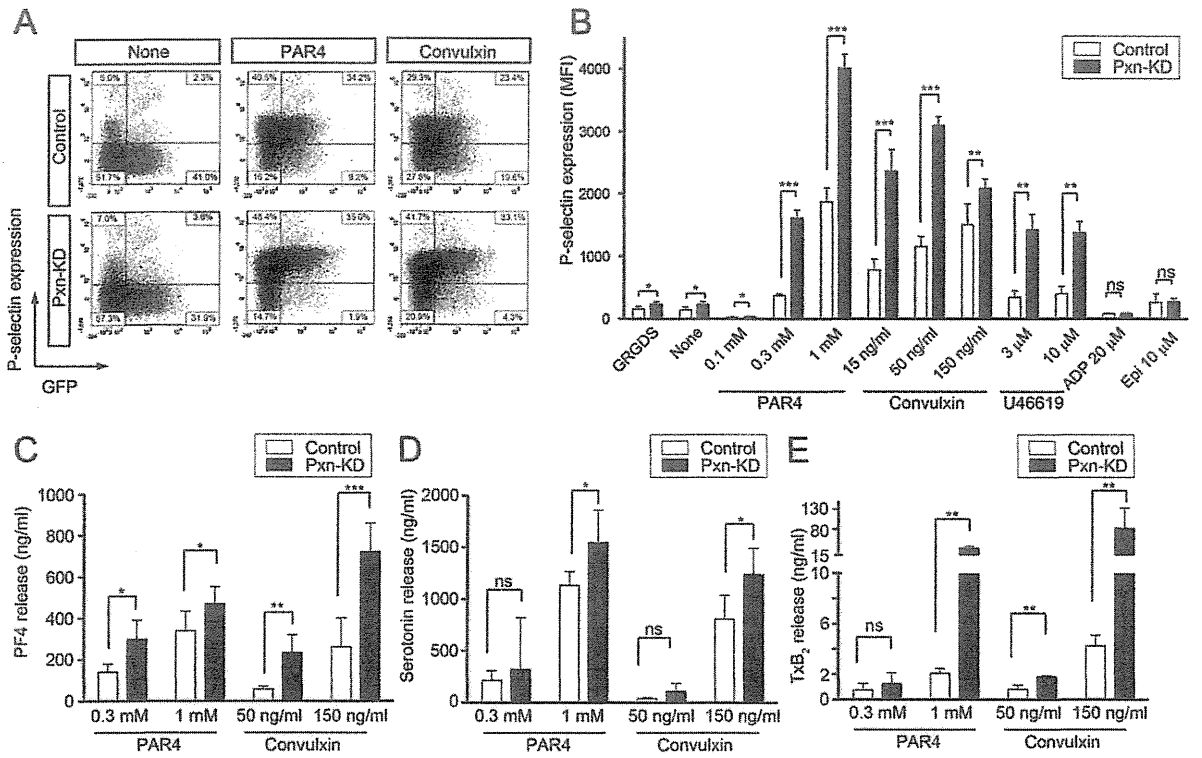

Figure 3 The release reaction is enhanced in Pxn-KD platelets. Bone marrow cells transduced with LentiLox-sh-control-GPIbα (Control) or LentiLox-sh-paxillin-GPIbα (Pxn-KD) at an MOI of 5 were transplanted into lethally irradiated recipient mice. **(A)** P-selectin expression on GFP-positive platelets stimulated with or without 1 mmol/L AYPGKF or 50 ng/mL convulxin was assessed by flow cytometry. The plots represent the degree of GFP expression (horizontal) and P-selectin expression (vertical). **(B)** Columns and error bars represent the mean ± s.d. of P-selectin expression after stimulation in GFP-positive platelets ($n = 3$–5). (C–E) Washed platelets were stimulated with the indicated agonist for 15 min, and then the concentrations of PF4 **(C)**, serotonin **(D)**, and TxB_2 **(E)** were measured in the supernatants. Columns and error bars represent the mean ± s.d. ($n = 5$). Open bars: control platelets; black bars: Pxn-KD platelets. Statistical significance was determined using Student's *t*-test. $^*P < 0.05$, $^{**}P < 0.01$, and $^{***}P < 0.001$ vs. control.

secondary effects of platelet aggregation, influx of extracellular calcium, and release reactions, we preincubated the platelets with EDTA, apyrase, and SQ29548. Intracellular calcium mobilization induced by the GPVI agonist convulxin and G protein-coupled receptor stimulation with AYPGKF was rather decreased by Pxn-KD (Figure 5B). These data suggest that paxillin targets downstream signaling of calcium mobilization or a calcium-independent signaling pathway.

To explore the importance of calcium-independent signaling pathways in Pxn-KD platelets, we employed BAPTA-AM, an intracellular calcium chelator, to exclude the effect of calcium mobilization. Because JON/A requires extracellular calcium for antibody binding, we assessed P-selectin expression induced by an agonist. Pretreatment with BAPTA-AM significantly suppressed P-selectin expression in both control and Pxn-KD platelets (Figure 5C). On the other hand, P-selectin expression elicited by an agonist was still observed in Pxn-KD platelets even in the presence of BAPTA-AM (Figure 5C). These data indicate that downstream signaling from intracellular calcium mobilization is amplified by Pxn-KD, and the calcium-independent pathway is activated by Pxn-KD to increase platelet activation.

Pxn-KD augments platelet adhesion and thrombus formation in vivo

Finally, we examined the contribution of paxillin to thrombus formation in vivo. To visualize thrombus formation in vivo, we used a direct visual technique based on confocal microscopy in mesenteric capillaries [26]. Thrombus formation in this system was initiated by the production of ROS following laser irradiation [26]. Laser irradiation-induced thrombus formation was significantly enhanced in Pxn-KD platelets (Figure 6A and 6B and Additional files 6 and 7). In addition, there was an enhancement of thrombus formation initiated by $FeCl_3$ in large femoral arteries (Additional file 8). Moreover, bleeding times after tail clipping significantly shortened in Pxn-KD experiments (Figure 6C). These findings support

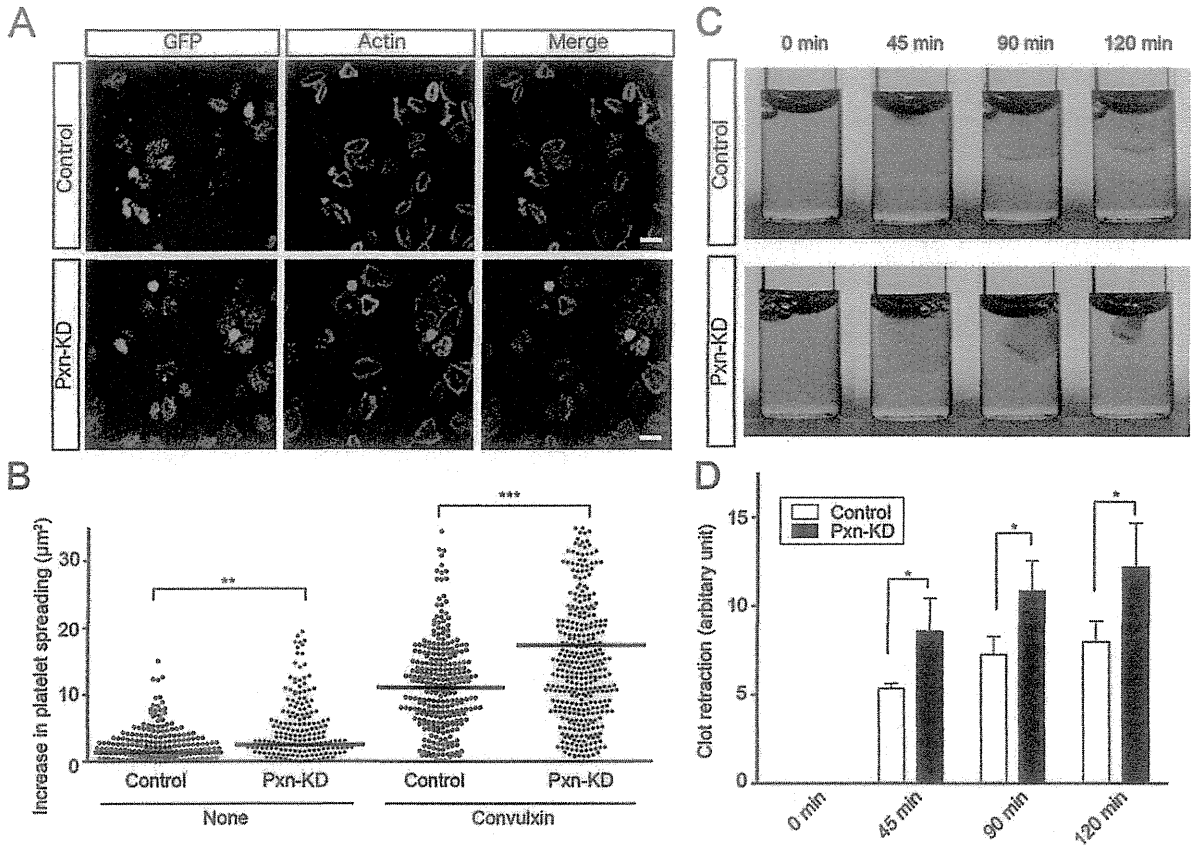

Figure 4 Pxn-KD platelets exhibit augmented outside-in signaling. (A) Control and Pxn-KD platelets treated with 50 ng/mL convulxin were allowed to adhere on immobilized fibrinogen for 30 min. The platelets were then fixed and stained with an anti-GFP antibody (green; left panel) and rhodamine-conjugated phalloidin (red; middle panel). The merged images show colocalization of GFP and actin staining (yellow; right panel). Original magnification, ×600; Bar, 5 μm. Data are representative of three independent experiments. **(B)** Platelets treated with or without 50 ng/mL convulxin were incubated in dishes coated with 400 μg/mL fibrinogen for 30 min. The area of cell spreading was quantified by ImageJ software. The mean platelet size on BSA was subtracted from the total spread area on fibrinogen to determine the actual increase in platelet spreading. The horizontal bar denotes the mean, and each symbol denotes an individual cell ($n = 281–394$ cells). **(C)** Clot retraction of platelet-rich plasma consisting of diluted human plasma and control or Pxn-KD platelets was initiated by 0.1 U/mL thrombin and then photographed at 0, 45, 90, and 120 min. **(D)** Clot retraction was quantified by measuring serum formation extruded by clot retraction. Columns and error bars represent the mean ± s.d. ($n = 3$). Open bars: control platelets; black bars: Pxn-KD platelets. Statistical significance was determined using Student's *t*-test. $^{*}P < 0.05$, $^{**}P < 0.01$, and $^{***}P < 0.001$ vs. control.

our hypothesis that paxillin is an important negative regulator of platelet activation and thrombus formation in vivo.

Discussion

Here, we found that the LIM protein paxillin is a negative regulator of platelet activation in mice. The negative regulation of platelet activation by paxillin was not limited to a specific signaling pathway, because Pxn-KD enhanced platelet activation in response to a variety of agonists. We also confirmed that thrombus formation was augmented in Pxn-KD platelets in vivo. This finding is notable because several previous reports suggest that changes in paxillin function actually reduce integrin signaling [13,14]. Furthermore, a previous finding in platelets has demonstrated the possible role of paxillin as a negative feedback regulator after integrin ligation to regulate the activity of Lyn tyrosine kinase [17]. However, this mode of regulation cannot fully explain the phenotypes of Pxn-KD platelets, because both outside-in and inside-out signaling were augmented by Pxn-KD. Our results reveal a new cellular function of paxillin and indicate new mechanisms that modulate platelet activation.

The most interesting result of this study was that Pxn-KD significantly enhanced the upstream signaling pathways that converge on platelet activation. Appropriate inhibition of the platelet response is essential to control pathological thrombus formation. It is well known that the mediators that enhance intracellular cAMP or cGMP

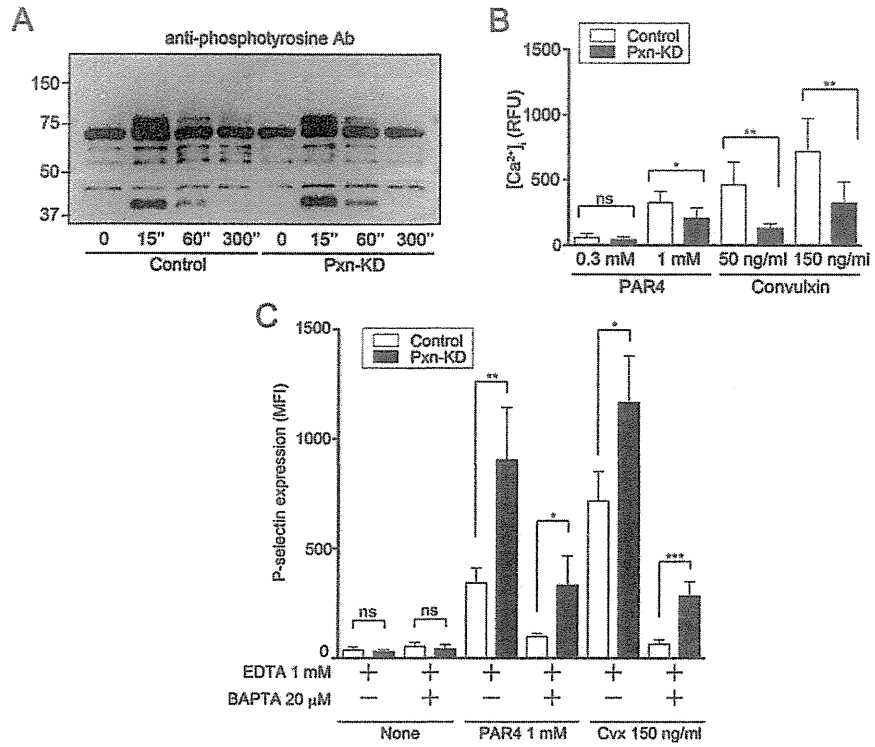

Figure 5 Pxn-KD fails to increase tyrosine phosphorylation and calcium mobilization. (A) Washed platelets obtained from control and Pxn-KD experiments were stimulated with 150 ng/mL convulxin for the indicated times. The cell lysates were resolved by SDS-polyacrylamide gel electrophoresis and then immunoblotted with an anti-phosphotyrosine mAb (4G10). The data shown are representative of three independent experiments. **(B)** Control and Pxn-KD platelets were labeled with GFP-Certified™ FluoForte™ dye. Changes in intracellular calcium levels after stimulation with an indicated concentration of AYPGKF or convulxin were then measured every 30 s. Data are expressed as the relative fluorescence unit (RFU) measured using a microplate spectrofluorometer (excitation, 530 nm; emission, 570 nm). The peak calcium concentration was measured after stimulation (open bars: control platelets; black bars: Pxn-KD platelets). Columns and error bars represent the mean ± s.d. (n = 5–8). Statistical significance was determined by the Student's t-test. **(C)** Control and Pxn-KD platelets were pretreated with 1 mmol/L EDTA and/or 20 μmol/L BAPTA-AM for 10 min, and then stimulated with or without 1 mmol/L AYPGKF or 150 ng/mL convulxin. P-selectin expression on GFP-positive platelets was determined by flow cytometry. Columns and error bars represent the mean ± s.d. of P-selectin expression (n = 4).

levels, including prostacyclin, prostaglandin E_1, and nitric oxide, are strong extrinsic inhibitors of platelet activation [27]. These extrinsic mediators ameliorate the broad platelet activation elicited by various agonists [27]. Intrinsic negative regulators of platelet activation have been identified recently, but many of these proteins only control a specific receptor signaling pathway. GPVI-mediated immunoreceptor tyrosine-based activation motif (ITAM) signaling is regulated by immunotyrosine-based inhibitory motif (ITIM)-containing receptors including platelet endothelial cell adhesion molecule 1 and carcinoembryonic antigen-related cell adhesion molecule 1 [28,29]. Furthermore, Lyn tyrosine kinase has been reported to inhibit ITAM signaling by inducing tyrosine phosphorylation of ITIM [28]. It has also been reported that binding of a regulator of G-protein signaling to the Giα subunit limits platelet responsiveness to the receptor, which is independent of Rap1b [30]. Conversely, paxillin may downregulate platelet activity by modulating a common pathway, because Pxn-KD resulted in marked platelet hyperactivation in response to stimulation of tyrosine phosphorylation-based receptors and G protein-coupled receptors.

Although paxillin is reportedly involved in various integrin-mediated cellular functions, many of these functions are limited to outside-in signaling pathways. Paxillin-deficient embryos show embryonic lethality, and the phenotype closely resembles that of fibronectin-deficient mice [31]. Moreover, paxillin-deficient fibroblasts show reductions in cell migration and tyrosine phosphorylation following cell adhesion [31]. Chimeric integrin αIIbβ3 with a cytoplasmic tail substitution of α4β1 or α9β1, which facilitates paxillin binding, significantly inhibits cell spreading, but does not affect αIIbβ3-dependent cell adhesion [18,19]. Inhibition of paxillin binding to integrin α4 inhibits leukocyte recruitment to an inflammatory site [32]. These data suggest important roles of paxillin in outside-in signaling by direct interaction with the integrin α-subunit. However, in this study, inside-out and outside-

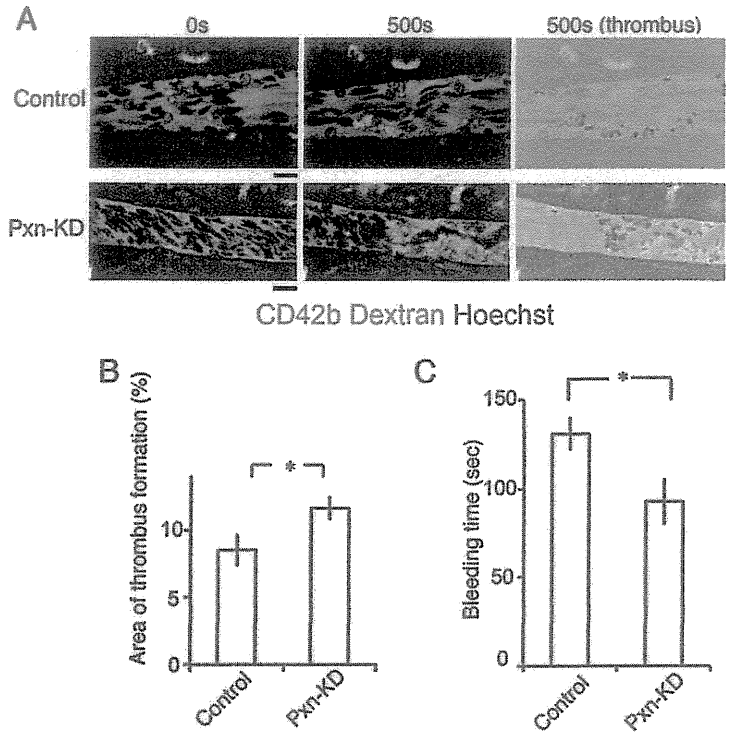

Figure 6 Pxn-KD in platelets expedites thrombus formation in vivo. (A) Intravital imaging of thrombus formation by laser irradiation of mesenteric arterioles in mice with control or Pxn-KD platelets. Thrombus formation was increased in mice with Pxn-KD platelets following laser irradiation. Bar, 10 μm. The right panel shows the results of quantification of the thrombus area. **(B)** Percentage areas of thrombus within blood vessels after laser irradiation. Columns and error bars represent the mean ± s.e.m. ($n = 40$ vessels in five mice/group). **(C)** Tail bleeding times were assessed as described in the Methods. Columns and error bars represent the mean ± s.e.m. (n = four mice/group). Statistical significance was determined using Student's *t*-test. $^*P < 0.05$ vs. control.

in signaling of integrin αIIbβ3 were increased in Pxn-KD platelets, even though paxillin failed to interact with platelet-specific integrin αIIb [19]. It is possible that other signaling pathways in platelets are modulated by paxillin, which is independent of direct interactions with integrins.

An issue that remains unresolved is the precise mechanism governing the negative regulatory function of paxillin in platelet activation. As described above, Rathore et al. previously reported that integrin αIIbβ3-dependent platelet aggregation induced tyrosine phosphorylation of paxillin and Hic-5 in platelets, leading to the binding of Csk, which controls activation of the Src family of tyrosine kinases [17]. Csk preferentially binds to paxillin in murine platelets that coexpress paxillin and Hic-5 [17]. Furthermore, the interaction abolishes the activity of Lyn, but not Fyn or Src. It is possible that paxillin acts as a negative feedback regulator of outside-in signaling by modulating Lyn activity after ligand binding to integrin αIIbβ3 [17]. However, this mechanism does not fully explain the functional roles of paxillin in platelets. Our data suggest that paxillin controls additional proximal signaling pathways for platelet activation. Pxn-KD did not directly augment the conformational changes of integrin αIIbβ3 expressed on Chinese hamster ovary cells (Additional file 9), tyrosine phosphorylation, or calcium mobilization induced by phosphoinositide turnover. These data suggest that paxillin negatively controls downstream signaling of calcium mobilization or a calcium-independent signaling pathway. In addition, calcium mobilization was rather reduced by Pxn-KD. It is therefore possible that negative feedback exists to prevent further activation of Pxn-KD platelets, or phosphoinositide turnover is directly modulated by Pxn-KD.

Our data suggest that several mechanisms may increase platelet activation by Pxn-KD. Notably, calcium-independent actions by Pxn-KD appear to exist, because P-selectin expression elicited by an agonist was still observed in Pxn-KD platelets even in the presence of BAPTA-AM. A previous report has suggested that coordinated signaling through both $G_{12/13}$ and G_i causes integrin αIIbβ3 activation, despite a small increase in intracellular calcium [33]. In addition, $G_{12/13}$ and G_i signaling activates integrin αIIbβ3 in Gq-deficient mice [34]. It is possible that paxillin modify the calcium-independent signaling

pathway leading to release reaction and integrinαIIbβ3 activation. Additional studies are needed to investigate how paxillin regulates platelet activation, and to assess whether these roles of paxillin in control of cellular signaling are common mechanisms in other cell types. We are now interested in further investigation of the precise mechanisms, and additional experiments are currently underway in our laboratory.

Another interesting finding of our study is that Pxn-KD resulted in an enlargement of platelet volume. CLP36, a member of the LIM domain family, was recently reported to play some roles in platelet activation [35]. Platelets from mice lacking the LIM domain of CLP36 show a slight increase in size and hyperactivation in response to a GPVI agonist [35]. The phenotypes of CLP36-deficient or mutant platelets are similar to those of Pxn-KD platelets in our study, although G protein-coupled receptor signaling is not affected in CLP36-deficient or mutant mice. Accordingly, the expression of LIM domain proteins may determine platelet size and reactivity.

To extrapolate the implications of our study to the biology and pathophysiology of humans, we must consider the differential expression pattern of paxillin-related proteins in platelets among species. Murine platelets express paxillin, Hic-5, and leupaxin, whereas human platelets only express Hic-5 [17]. Hagmann et al. reported that a switch from paxillin to Hic-5 expression should occur during the late phase of megakaryopoiesis in humans [15]. A recent report has described platelet functions in Hic-5-deficient mice [36]. Hic-5-deficient mice exhibit prolonged bleeding times, and the loss of Hic-5 in platelets slightly impairs integrin αIIbβ3 activation induced by thrombin, but not other agonists including convulxin, U46619, and ADP [36]. Although the hemostatic defect in Hic-5-deficient mice, as assessed by tail bleeding, is not fully explained by a mild defect in platelet function, it is possible that the structurally related proteins paxillin and Hic-5 play opposing roles in the regulation of platelet function in murine platelets. Leupaxin, another LIM protein that is predominantly expressed in leukocytes, has been reported to play an inhibitory role in B cell receptor signaling [37], which is similar to the role of paxillin reported in this study. In human platelets, which only express Hic-5, it will be necessary to elucidate whether Hic-5 acts as a positive regulator of integrin αIIbβ3 activation.

In summary, we have shown that paxillin is a negative regulator of platelet activation in mouse platelets. Modulation of platelet activation by Pxn-KD may originate in the augmentation of common signaling pathways, leading to integrin αIIbβ3 activation, release reactions, and Tx biosynthesis. Modulation of the LIM protein function might be an attractive candidate therapeutic target capable of strongly suppressing unexpected platelet activation in thrombotic disorders. The next challenge will be elucidating the precise mechanism by which paxillin regulates the signaling pathway in platelet activation.

Additional files

Additional file 1: Schematic diagrams of the lentiviral vector used in this study. (A) Schematic diagram of the lentiviral vector. (B) Locations of the oligonucleotides encoding the shRNAs in the mouse *paxillin* (*Pxn*) gene. (C) Mouse embryonic fibroblasts were transduced with a lentiviral vector containing the control, Pxn-1, Pxn-2, or Pxn-3 shRNA sequences at MOIs of 1, 3, or 10. Protein expression was determined by immunoblotting at 48 h after transduction. Data are representative of three independent experiments.

Additional file 2: Oligonucleotide sequences of siRNA cloned into LentiLox.

Additional file 3: Pxn-KD does not affect granule contents. Bone marrow cells transduced with LentiLox-sh-control-GPIbα (Control) or LentiLox-sh-paxillin-GPIbα (Pxn-KD) at an MOI of 5 were transplanted into lethally irradiated recipient mice. (A) The morphology of control and Pxn-KD platelets was examined by transmission electron microscopy, and the areas of granules and cytoplasm in each platelet were independently quantified using ImageJ software for Macintosh. Columns and error bars represent the mean ± s.d. ($n = 53–70$). (B–C) Washed platelets were lysed to measure the concentrations of platelet factor 4 (PF4) (B) and serotonin (C). Columns and error bars represent the mean ± s.d. ($n = 4$). Statistical significance was determined using Student's t test. $^{***}P < 0.001$ vs. control.

Additional file 4: Expression levels of platelet-specific glycoproteins. Description of data: (A) Expression levels of GPIIb/IIIa (integrin αIIbβ3) (left panel), GPIb (middle panel), and GPVI (right panel) in control (dark gray) and paxillin-knockdown platelets (light gray). (B) Columns and error bars represent the mean ± s.d. of the mean fluorescence intensity (MFI) of antibody binding ($n = 5$). Statistical significance was determined using Student's t test. $^{*}P < 0.05$, $^{**}P < 0.01$, and $^{***}P < 0.001$ vs. control.

Additional file 5: Effects of apyrase and SQ29548 on agonist-induced integrin αIIbβ3 activation and P-selectin expression in control and Pxn-KD platelets. Platelets pretreated without or with 5 U/mL apyrase and 10 μmol/L SQ29548 were stimulated with the indicated agonists. JON/A binding (A) and P-selectin expression (B) on GFP-positive platelets were assessed by flow cytometry. Column and error bars represent the mean ± s.d. of the mean fluorescence intensity (MFI) ($n = 3–4$). Statistical significance was determined using Student's t test. $^{*}P < 0.05$, $^{**}P < 0.01$, and $^{***}P < 0.001$ vs. control.

Additional file 6: Intravital imaging of thrombus formation by laser irradiation of mesenteric arterioles in mouse with control platelets.

Additional file 7: Intravital imaging of thrombus formation by laser irradiation of mesenteric arterioles in mice with Pxn-KD platelets.

Additional file 8: Thrombus formation in femoral arteries induced by FeCl3. (A) Intravital imaging of thrombus formation 5 mins after FeCl3 treatment in femoral arteries in mice with control or paxillin knock-down platelets (Pxn-KD). The black arrows indicate the direction of blood flow, and triangles show the developed thrombus. Bar, 100 μm. (B) Areas of thrombus within arteries 20 mins after laser irradiation. Columns and error bars represent the mean ± s.e.m. (n = 8 arteries in four mice/group).

Additional file 9: Knock-down of paxillin does not affect talin-dependent activation of integrin αIIbβ3 in CHO cells. (A) Schematic representation of the lentiviral vectors used in this experiment. (B–D) αIIbβ3-CHO cells were transduced with lentiviral vectors expressing a control shRNA sequence and GFP (Control), the paxillin shRNA sequence and GFP (Pxn-KD), a control shRNA sequence and the GFP-Talin FERM domain (Control-FERM), or the paxillin shRNA sequence and the GFP-Talin FERM domain (Pxn-KD-FERM). (B) Lysates obtained from the transduced cells were immunoblotted with anti-GFP polyclonal antibody, anti-paxillin monoclonal antibody, and anti-vinculin monoclonal antibody. (C) PAC-1 binding after transduction in the presence or absence of 1 mmol/L GRGDS was assessed by